# Photoreflectance, photoluminescence, and microphotoluminescence study of optical transitions between delocalized and localized states in $GaN_{0.02}As_{0.98}$, $Ga_{0.95}In_{0.05}N_{0.02}As_{0.98}$, and $GaN_{0.02}As_{0.90}Sb_{0.08}$ layers

R. Kudrawiec,[1,*] M. Latkowska,[1] M. Baranowski,[1] J. Misiewicz,[1] L. H. Li,[2,†] and J. C. Harmand[2]
[1]*Institute of Physics, Wroclaw University of Technology, Wybrzeże Wyspiańskiego 27, 50-370 Wrocław, Poland*
[2]*Laboratoire de Photonique et de Nanostructures, CNRS Route de Nozay, 91460 Marcoussis, France*
(Received 28 May 2012; revised manuscript received 12 May 2013; published 3 September 2013)

Optical transitions in as-grown and annealed $GaN_{0.02}As_{0.98}$, $Ga_{0.95}In_{0.05}N_{0.02}As_{0.98}$, and $GaN_{0.02}As_{0.90}Sb_{0.08}$ bulklike layers have been studied with photoreflectance (PR), photoluminescence (PL), and microphotoluminescence ($\mu$PL) in a broad range of temperatures. The exciton binding energy and the temperature dependence of the energy gap have been determined from PR measurements. In addition, the alloy-related broadening of optical transitions has been analyzed and compared for the three alloys. The largest alloy inhomogeneities have been observed for $GaN_{0.02}As_{0.90}Sb_{0.08}$. In $\mu$PL spectra of $GaN_{0.02}As_{0.98}$ and $Ga_{0.95}In_{0.05}N_{0.02}As_{0.98}$ layers measured at low temperatures and low excitation conditions, sharp PL lines of 100–300-$\mu$eV widths have been clearly observed ~10–20 meV below the energy gap of these alloys. Analyzing the temperature quenching of the sharp PL lines, they have been attributed to the recombination of localized excitons trapped at deep donor (acceptor)-like states. Such lines were not well resolved for $GaN_{0.02}As_{0.90}Sb_{0.08}$ layers. The analysis of thermal quenching of localized exciton emission suggests that for this alloy excitons are localized mostly on alloy content fluctuations. With the increase in the excitation power an additional PL band has been observed in $\mu$PL spectra at the higher-energy side. This band corresponds to the optical transitions between delocalized states which are observed in photoreflectance spectra. The emission of localized excitons without resolved sharp lines has been also observed with macro-PL measurements at low temperatures. In addition, the donor trap–valence band (DT-VB) recombination has been identified for the three alloys in macro-PL spectra. It has been clearly observed that the intensity of DT-VB recombination is the weakest for $GaN_{0.02}As_{0.90}Sb_{0.08}$ alloys whereas for $GaN_{0.02}As_{0.98}$ and $Ga_{0.95}In_{0.05}N_{0.02}As_{0.98}$ alloys it is very similar. The observed differences between the three alloys and the role of postgrowth annealing have been analyzed and discussed in the context of the influence of III-V host on alloy inhomogeneities, formation of native point defects in III-V-N alloys, and their influence on the optical quality of III-V-N alloys.

DOI: 10.1103/PhysRevB.88.125201 PACS number(s): 78.20.Bh, 78.55.Cr

## I. INTRODUCTION

The incorporation of a few percent of nitrogen atoms into III-V host leads to a remarkable band-gap reduction which appears mainly in the conduction band.[1–4] Because of this feature III-V-N alloys (so-called dilute nitrides) are very promising candidates for various optoelectronic applications including solar cells and GaAs-based telecommunication laser diodes.[2,5–7] Unfortunately the incorporation of nitrogen also deteriorates the optical quality of the III-Vs by inducing carrier localization at low temperatures and strong nonradiative recombination at room temperature. The issue of material degradation with the increase of nitrogen concentration is one of the most important research aspects of this material system from the viewpoint of its application in solar cells and diode lasers. Rapid thermal annealing is widely employed to improve the optical quality of dilute nitrides. The annealing process removes a significant part of nonradiative centers; however, the low-temperature photoluminescence (PL) measured at low excitation conditions is still dominated by the recombination of localized carriers (excitons) trapped at local potential minima.[8,9] Currently, it is widely accepted that the PL band attributed to the recombination of localized excitons is composed of sharp lines. This conclusion is supported by near-field photoluminescence[10–12] and microphotoluminescence ($\mu$PL) measurements[13–15] of GaNAs and GaInNAs layers. However the exact nature of the narrow exciton lines is still under debate. Alloy composition fluctuations creating local potential minima represent a possible origin for exciton localization. This explanation was strongly supported for the GaInNAs alloy[11] for which compositional fluctuations were indeed observed.[16] Quite recently it has been also observed that the dispersion of localization energy for GaInNAs alloys can be very large (~0–150 meV) whereas all the individual lines have a similar activation energy which is close to the electron-hole attraction in this system (i.e., ~6 meV).[15] It suggests that these sharp PL lines observed at low temperatures correspond to recombination of excitons localized on deep donor- or acceptor-like states which lie within the energy gap. When the thermal energy becomes higher that the exciton binding energy, the deep centers trap individual carriers which recombine non radiatively.[15] Since the effect of nonradiative recombination is enhanced for larger nitrogen concentrations it is expected that N-related point defects can be responsible for the carrier localization phenomenon and the poor optical quality of III-V-N alloys. Moreover, it is very likely that the same nitrogen concentration should influence the structural and optical quality of various III-V alloys differently. Indeed the impact of N incorporation strongly depends on the composition of the host material. Careful comparative studies on this issue have not been reported so far. It is worth noting that the PL technique is particularly inappropriate to measure the temperature dependence of the band-gap energy of III-V-N alloys due to this strong carrier localization.[17–22]

 ©2013 American Physical Society

Therefore, investigations on temperature dependence of the energy $[E_0(T)]$ and broadening parameter $[\Gamma_0(T)]$ of the fundamental band gap for III-V-N alloys are necessary to clarify the issue of localized and delocalized states in various III-V-N.

In this work, we apply photoreflectance (PR) combined with microphotoluminescence ($\mu$PL) spectroscopy to study the optical transitions in as-grown and annealed $GaN_{0.02}As_{0.98}$, $Ga_{0.95}In_{0.05}N_{0.02}As_{0.98}$, and $GaN_{0.02}As_{0.90}Sb_{0.08}$ epitaxial layers of the same nitrogen concentration ($N = 2\%$) focusing on the role of III-V host in the optical quality of III-V-N alloys. We show that the PL band attributed to the recombination of localized carriers is clearly composed of individual sharp PL lines, the nature of which is discussed in this work. In addition, we determine the temperature dependence of the energy and broadening parameter of the fundamental band gap for the three alloys by using the PR technique, which is insensitive to localized states and probes optical transitions between extended states (i.e., free excitonic transitions and energy-gap transitions). The obtained $E_0(T)$ and $\Gamma_0(T)$ characteristics are discussed in the context of the same nitrogen incorporation in different III-V hosts. Since the band structure and optical properties of dilute nitrides strongly depend on nitrogen concentration the set of three samples with the same nitrogen concentration is representative to discuss the influence of III-V host on properties of dilute nitrides.

## II. EXPERIMENT

The samples were grown by molecular beam epitaxy on semi-insulating (100) GaAs substrates. They consist of a 120-nm-thick GaAs buffer layer followed by 100-nm-thick $GaN_{0.02}As_{0.98}$, $Ga_{0.95}In_{0.05}N_{0.02}As_{0.98}$ or $GaN_{0.02}As_{0.90}Sb_{0.08}$ layers and are capped by 20 nm of GaAs. The content of the layers was determined on the basis of secondary ion mass spectroscopy and high-resolution x-ray diffraction (HRXRD) investigations. The annealing process was conducted at 750 °C for 10 min. The structural properties of the samples were carefully compared before and after annealing. HRXRD measurements did not reveal any changes of the average composition of these samples due to annealing. In addition, transmission electron microscopy (TEM) did not show any significant alloy fluctuations or clustering phenomena, suggesting that composition uniformity was not affected by annealing.[23] Therefore it can be considered that the average layer content is the same before and after annealing. Moreover, it is worth noting that the present study is not based on quantum wells but on relatively thick layers (0.1 $\mu$m). Therefore the possible interdiffusion of the constituents at the layer interfaces is not expected to affect the optical properties of these samples.

A "bright configuration" of the experimental setup was used to measure the PR spectra. In this configuration the sample is illuminated by white light from the halogen lamp and next the reflected light is dispersed through the monochromator.[24] A single-grating 0.55-m focal length monochromator and a thermoelectrically cooled InGaAs *pin* photodiode were used to disperse and detect the reflected light from the samples. As the probe and pump sources, a 150-W tungsten-halogen and a He-Ne laser were used, respectively. The probe and pump beams were focused onto the sample to the diameter of 1–2 mm and the power of the probe beam was reduced to 0.1 mW using a gray filter. The pump beam was modulated by a mechanical chopper with the frequency of 280 Hz. Phase-sensitive detection of the PR signal was made using a lock-in amplifier. For temperature-dependent PR measurements samples were mounted on a cold finger in a helium closed cycle refrigerator coupled with a programmable temperature controller allowing measurements in the 10–320 K temperature range.

Microphotoluminescence ($\mu$PL) spectra were measured using a single-grating 0.55-m focal length monochromator with a multichannel InGaAs detector. The 660-nm line of a semiconductor laser was focused on the sample by a long working distance objective. The diameter of the laser spot was estimated to be below 2 $\mu$m. For measurements, samples were mounted on a cold finger in a helium flow cryostat coupled with a programmable temperature controller allowing measurements in the 2–320 K temperature range.

## III. RESULTS AND DISCUSSION

In order to study optical transitions between delocalized and localized states in $GaN_{0.02}As_{0.98}$, $Ga_{0.95}In_{0.05}N_{0.02}As_{0.98}$ and $GaN_{0.02}As_{0.90}Sb_{0.08}$ layers and discuss the influence of the host matrix on the optical quality of these layers, careful PR, PL, and $\mu$PL measurements have been performed for the three layers at the same conditions in a broad range of temperatures. First, low-temperature PR and PL measurements are compared for these layers; next, temperature dependences of the energy gap extracted from PR measurements are analyzed; and finally $\mu$PL spectra obtained at various excitation conditions and temperatures are presented and discussed. In order to support conclusions from $\mu$PL measurements, Monte Carlo simulations of hopping excitons in III-V-N alloys with various concentrations of localizing centers have been performed.

### A. Photoreflectance versus macrophotoluminescence

Figure 1 shows PR and macro-PL spectra measured for as-grown and annealed $GaN_{0.02}As_{0.98}$, $Ga_{0.95}In_{0.05}N_{0.02}As_{0.98}$, and $GaN_{0.02}As_{0.90}Sb_{0.08}$ layers at low temperature. The energy gap of these layers can be determined from the analysis of PR spectra since these spectra are not sensitive to localized states and exhibit optical transitions between extended states (i.e., free excitonic transitions and/or band-to-band transitions). It is worth noting that the shape of PR resonances is different for the three samples. This shape can be tuned by the detection phase on the lock-in amplifier. It does not influence the energy of optical transition and is a well known feature of PR spectroscopy. The energy gap is marked in Fig. 1 by a dashed vertical line for each sample. It is clearly visible that for the three alloys the energy gap shifts to blue due to annealing. This phenomenon is well known for dilute nitrides and is associated with the opening of the energy gap due to atom reordering after annealing.[25–28] This reordering must be very local since no structural changes were observed by HRXRD or TEM.

In PL spectra, three PL bands can be distinguished for the three alloys. For as-grown $GaN_{0.02}As_{0.98}$ and $Ga_{0.95}In_{0.05}N_{0.02}As_{0.98}$ layers a broad PL band is observed at ~0.85 eV. Recently very similar emission was observed for GaNAs layers of various nitrogen concentrations.[29] For

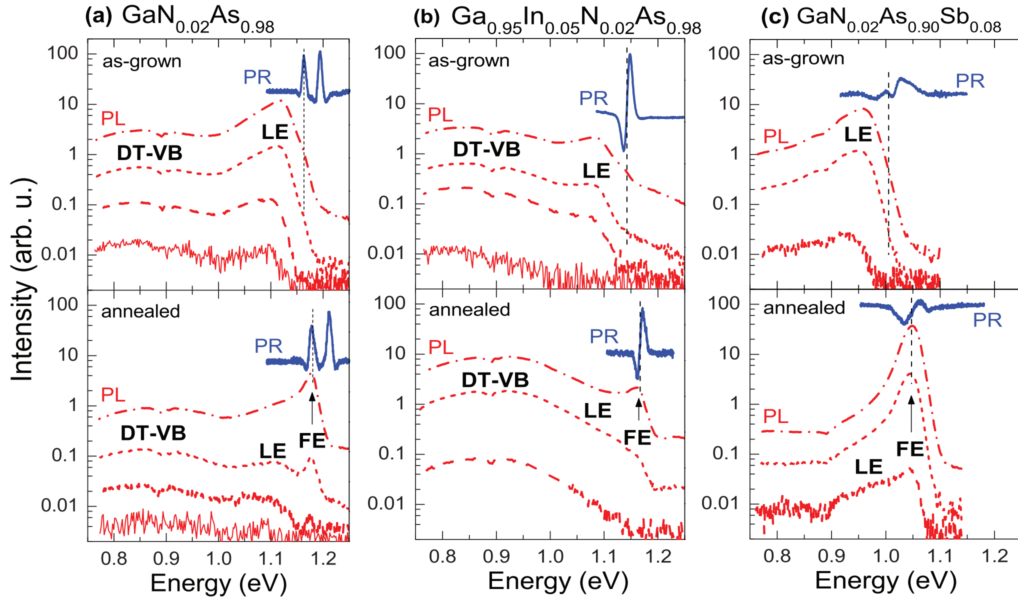


FIG. 1. (Color online) PR and macro-PL spectra measured at 10 K for as-grown and annealed (a) $GaN_{0.02}As_{0.98}$, (b) $Ga_{0.95}In_{0.05}N_{0.02}As_{0.98}$, and (c) $GaN_{0.02}As_{0.90}Sb_{0.08}$ layers. The excitation intensity for macro-PL measurements is 7.5, 0.54, 0.24, and 0.08 W/cm$^2$ for dash-dot, short-dashed, dashed, and solid lines, respectively.

these layers deep-level transient spectroscopy (DLTS) measurements were performed and the broad PL band located at this energy has been attributed to the donor trap–valence band (DT-VB) recombination between deep electron traps identified in DLTS measurements. It is expected that the origin of the PL band observed at ~0.85 eV for $GaN_{0.02}As_{0.98}$ and $Ga_{0.95}In_{0.05}N_{0.02}As_{0.98}$ layers is like that in Ref. 29 and, therefore, this emission is attributed to DT-VB recombination. The PL band related to DT-VB recombination is rather not observed for $GaN_{0.02}As_{0.90}Sb_{0.08}$ or its intensity is much weaker in this case than in the two previous samples. This indicates a better optical quality of the $GaN_{0.02}As_{0.90}Sb_{0.08}$ alloy, further evidenced by the strong intensity of the free exciton (FE) and/or band-to-band emission observed for this alloy (see FE label in Fig. 1). For the three alloys, this emission is clearly visible only after annealing and at high-enough excitation power. Before annealing, the PL spectra are dominated by an emission at lower energy which is attributed to localized excitonic (LE) recombination while the FE transition is very weak or even absent. Our interpretation of the three PL bands is supported by PR and $\mu$PL investigations presented below.

### B. Photoreflectance studies of temperature dependence of energy gap

Figures 2(a)–2(c) show PR spectra measured in the temperature range of 10–320 K for as-grown $GaN_{0.02}As_{0.98}$,

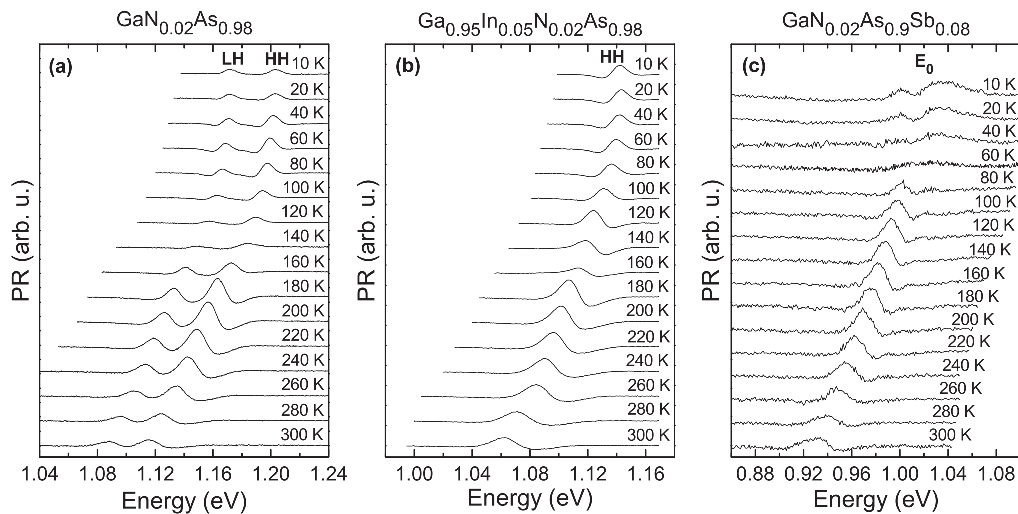


FIG. 2. Temperature dependence of PR spectra measured for as-grown (a) $GaN_{0.02}As_{0.98}$, (b) $Ga_{0.95}In_{0.05}N_{0.02}As_{0.98}$, and (c) $GaN_{0.02}As_{0.90}Sb_{0.08}$ layers.

$Ga_{0.95}In_{0.05}N_{0.02}As_{0.98}$, and $GaN_{0.02}As_{0.90}Sb_{0.08}$ layers, respectively. It is clearly visible that PR transitions shift to red and broaden with the increase in temperature. In addition, it is observed that the PR resonance intensity (i.e., the peak-to-peak amplitude) does not decrease monotonically with the temperature increase, which is an unusual observation for high-quality semiconductors. This effect is observed for these alloys since the band bending modulation in PR measurements is weaker at low temperatures due to the carrier localization phenomenon in these samples.[30]

Before the analysis of temperature dependence of energy gap in these samples it is worth noting that the three layers possess different strains as determined from HRXRD.[23] The $GaN_{0.02}As_{0.98}$ ternary layer is tensilely strained ($\varepsilon = -7.9 \times 10^{-3}$), and its PR spectra shown in Fig. 2(a) clearly exhibit two structures which are related to the heavy- and light-hole splitting. The PR resonance at the lower energy corresponds to the optical transition occurring between the light-hole band and the conduction band (LH transition). The second line at higher energy is associated with the absorption between the heavy-hole band and the conduction band (HH transition). The $Ga_{0.95}In_{0.05}N_{0.02}As_{0.98}$ layer is almost lattice matched to the GaAs substrate ($\varepsilon = -0.7 \times 10^{-3}$), and thereby unstrained. In consequence, no significant splitting of the valence band is expected for this sample, and a single structure is observed on the PR spectra. The $GaN_{0.02}As_{0.90}Sb_{0.08}$ layer is compressively strained ($\varepsilon = 4.5 \times 10^{-3}$) and, hence, a 15-meV valence band splitting is expected for this sample according to standard strain calculations in this material system; see, for example, Ref. 31. In general, the shape of PR resonance confirms the valence band splitting in this sample but the broadening of PR resonances related to heavy- and light-hole transitions is much larger than in the two previous samples and, therefore, the two transitions are not well separated in PR spectra. According to alloying rules, this larger PR resonance broadening is expected in this sample for two reasons. First, the Sb concentration (0.08) is larger than the In concentration (0.05) of the GaInNAs sample. Second, the band-gap bowing is stronger for alloys containing both N and Sb. For GaInAs the band-gap bowing equals 0.477 eV while for GaAsSb it is 1.43 eV.[32]

In order to determine energies and broadenings of optical transitions from PR measurements, these spectra were analyzed using the standard critical point (CP) model.[33] According to this model the PR spectrum can be fitted using the following formula:

$$\frac{\Delta R}{R} = \mathrm{Re}\left[\sum_{j=1}^{n} C_j e^{i\theta_j}(\hbar\omega - E_j + i\Gamma_j)^{-m_j}\right], \qquad (1)$$

where $n$ is the number of the spectral functions to be fitted; $\hbar\omega$ is the photon energy of the probe beam; $E_j$ is the CP energy; and $\Gamma_j$, $C_j$, and $\theta_j$ are the broadening, amplitude, and phase angle, respectively. The term $m_j$ refers to the type of CPs, i.e., the nature of optical transitions, namely: $m = 2$ and 2.5 for excitonic transition and band-to-band transition, respectively.

For the $GaN_{0.02}As_{0.98}$ layer it has been observed that at low temperature, each optical transition associated with LH and HH can be composed of two PR resonances: one related to excitonic and the other to band-to-band absorption.[34] Figure 3 compares the PR spectrum of the $GaN_{0.02}As_{0.98}$ layer measured at 60 K with different calculations. Attempts to fit the experimental spectra with two band-to-band transitions (short dashed line) or two excitonic transitions (dashed line) only are not fully satisfactory. In particular, the temperature dependence of the transitions in the 10–80 K range cannot be adequately reproduced by Varshni[35] or Bose-Einstein expressions[36] since the transition energy increases with the rise of temperature up to ~60 K that is unusual for these expressions. Such a variation of transition energy in this temperature range is observed since the character of PR resonance is excitonic at low temperature and becomes band to band with the rise of temperature. The agreement with Varshni and Bose-Einstein expressions is much improved when we consider that each of the LH and HH transitions consists of two contributions, the first related to excitonic absorption and the second related to band-to-band absorption (see the solid line in Fig. 3). The moduli of the individual PR resonances ($\rho$) have been obtained according to Eq. (2):

$$\Delta\rho_j(E) = \frac{|C_j|}{\left[(\hbar\omega - E_j)^2 + \Gamma_j^2\right]^{m_j/2}}, \qquad (2)$$

with parameters derived from the fit. The moduli are shown at the bottom of Fig. 3.

The splitting between the excitonic and band-to-band contributions, which is a direct measurement of the free exciton

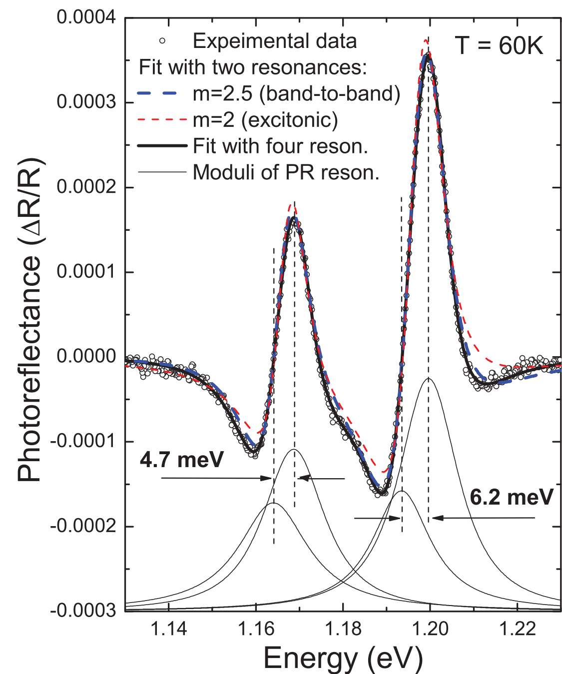


FIG. 3. (Color online) PR spectrum of as-grown $GaN_{0.02}As_{0.98}$ layer measured at 60 K (open points) together with different fitting curves. The short-dashed and dashed lines represent the fitting of PR data using two band-to-band ($m = 2.5$) and two excitonic ($m = 2$) resonances, respectively. The solid line represents the fit using four resonances, two excitonic and two band to band. The contribution of the individual PR resonances (i.e., their moduli) to the total approximating curve is presented at the bottom part of the figure. The correlation coefficient ($R^2$) is 0.954 and 0.972 for the fit by two resonances with $m = 2$ and 2.5, respectively, and 0.999 for the fit by four resonances (two with $m = 2$ and two with $m = 2.5$).

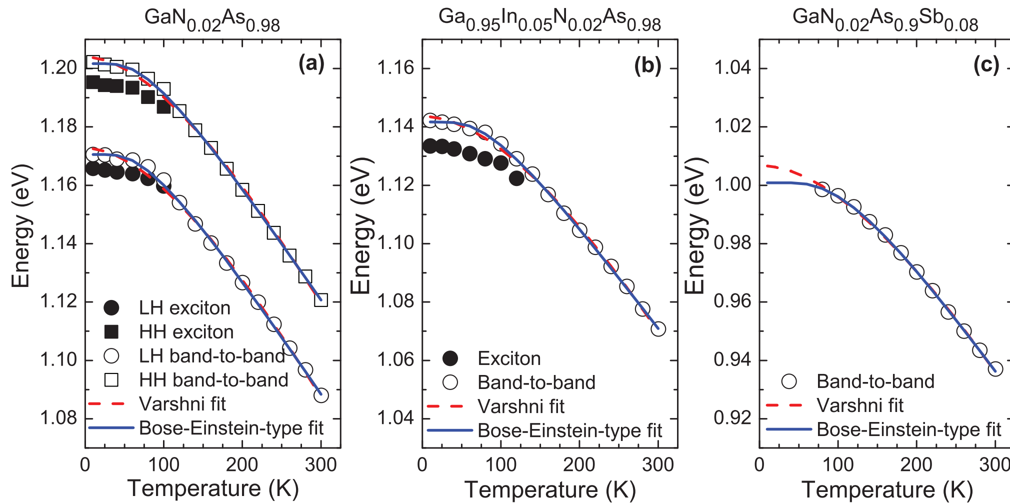


FIG. 4. (Color online) Temperature dependencies of energies of optical transitions (solid points: excitonic transitions; open points: band-to-band transitions) determined from PR measurements for as-grown (a) $GaN_{0.02}As_{0.98}$, (b) $Ga_{0.95}In_{0.05}N_{0.02}As_{0.98}$, and (c) $GaN_{0.02}As_{0.90}Sb_{0.08}$ layers. Dashes and solid lines correspond to fits by Varshni and Bose-Einstein formulas, respectively.

binding energy, can be extracted from our fitting procedure with four PR resonances. For the $GaN_{0.02}As_{0.98}$ layer, this can be done quite accurately between 40 and 100 K, because contributions of excitonic and band-to-band resonances are comparable in this temperature range. As the temperature increases, the contribution of excitonic resonance decreases. As a consequence, above 120 K, the fit with four resonances is no longer valid, but a satisfactory fit is obtained with two band-to-band transitions.

For the $Ga_{0.95}In_{0.05}N_{0.02}As_{0.98}$ layer, an excitonic contribution has been also identified at low temperature and, therefore, PR spectra have been fitted by two PR resonances: one related to an excitonic absorption and the second related to a band-to-band absorption.

PR spectra of the $GaN_{0.02}As_{0.90}Sb_{0.08}$ layer have been fitted by one resonance, which is attributed to HH transition. In this case an excitonic contribution to the PR signal is also expected at low temperatures, but the broadening of the PR feature is too large for a reasonable fitting of this signal by two or more resonances.

Figure 4 shows energies of excitonic and band-to-band transitions obtained from the fitting of PR spectra for the three samples. Two very valuable properties of these layers can be extracted from these data. The first property is the free exciton binding energy in $GaN_{0.02}As_{0.98}$ and $Ga_{0.95}In_{0.05}N_{0.02}As_{0.98}$ layers whereas the second one is the temperature dependence of the energy gap for the three alloys. Concerning the exciton binding energy it is worth noting that the observed reduction in energy separation between the excitonic and band-to-band resonance for $T > 80$ K [see solid and open points in Figs. 4(a) and 4(b)], does not mean a temperature-induced reduction of exciton binging energy in these alloys. This observation is associated with the fact that the contribution of the PR signal related to excitonic transition decreases with the increase in temperature. Therefore the exciton binding energy is determined at lower temperatures.

For $GaN_{0.02}As_{0.98}$ layer the LH and HH exciton binding energies have been determined to be $4.5 \pm 0.5$ and $6.5 \pm 0.5$ meV, respectively. These binding energies are much larger than the free exciton binding energy in GaAs. This phenomenon is mainly attributed to the nitrogen induced increase in the electron effective mass, which influences the exciton reduced mass $\mu$. Our experimental values correspond to a ~60% increase in comparison to the electron effective mass ($m_e$) in GaAs, which is 0.067 $m_0$ according to Ref. 32. The founded increase in the electron effective mass upon nitrogen incorporation is in good agreement with the study of the electron effective mass at the bottom of the conduction band in GaNAs/GaAs quantum wells where the electron effective mass was reported to be in the range of 0.09–0.12 $m_0$.[37,38]

Very similar exciton binding energy has been estimated for the $Ga_{0.95}In_{0.05}N_{0.02}As_{0.98}$ layer ($8 \pm 2$ meV). In this case this energy is attributed to the HH exciton since the PR signal related to this transition is stronger (see, for example, PR spectrum for the GaNAs layer). However, a contribution of the PR signal related to the LH transition cannot be excluded in this case and, therefore, the determination of the exciton binding energy is less accurate for this layer than for the ternary layer where the HH and LH transitions are well separated. So far the exciton binding energy has not been studied for bulk dilute nitrides. It is worth noting that the standard approach to determine the binding energy from the thermal quenching of free excitonic recombination is very limited in this case due to strong carrier localization at low temperatures. Moreover the other method based on measurements of excited states for free excitonic transitions in reflectance spectra, which is typical for binary semiconductors,[39,40] does not work in this case due to large broadening of excitonic transitions caused by the alloying effect.

The temperature dependencies of optical transitions related to band-to-band absorption have been fitted using both the Varshni[35] and Bose-Einstein-type[36] (B-E) expressions. The Varshni equation is given by

$$E_0(T) = E_0(0) - \frac{\alpha T^2}{\beta + T}, \tag{3}$$

TABLE I. Varshni and Bose-Einstein parameters extracted from fitting of PR data shown in Fig. 4 by Eqs. (3) and (4).

| Sample | $E_0(0)$ (eV) | $\alpha$ ($10^{-4}$ eV/K) | $\beta$ (K) | $E_0(0)$ (eV) | $a_B$ (meV) | $\Theta_B$ (K) |
|---|---|---|---|---|---|---|
| GaAs[a] | 1.519 | 5.4 | 225 | 1.571 | 57 | 240 |
| $GaN_{0.02}As_{0.98}$ | | | | | | |
| LH | 1.173 | 5.90 | 323 | 1.171 | 47.9 | 232 |
| HH | 1.204 | 5.89 | 329 | 1.202 | 47.9 | 234 |
| $Ga_{0.95}In_{0.05}N_{0.02}As_{0.98}$ | 1.144 | 5.99 | 432 | 1.142 | 47.6 | 256 |
| $GaN_{0.02}As_{0.90}Sb_{0.08}$ | 1.007 | 5.95 | 456 | 1.001 | 67.7 | 339 |

[a]Reference 41.

where $E_0(0)$ is the band gap at $T = 0$ K while $\alpha$ and $\beta$ are the so-called Varshni coefficients. The B-E expression, which involves electron coupling to an average phonon (optical and acoustical), is given by Eq. (4):

$$E_0(T) = E_0(0) - \frac{2a_B}{\exp\left(\frac{\Theta_B}{T}\right) - 1}, \tag{4}$$

where $a_B$ is the strength of the electron-average phonon interaction and $\Theta_B$ is the average phonon temperature.

The dashed and solid lines in Fig. 4 are fits to Eqs. (3) and (4), respectively. The fit-determined parameters, $E_0(0)$, $\alpha$, $\beta$, $a_B$, and $\Theta_B$, together with literature data for GaAs host[32,41] are listed in Table I.

Figure 5 shows temperature dependences of broadenings of PR resonances related to the band-to-band absorption. This dependence can be described by the Bose-Einstein formula,

$$\Gamma_0(T) = \Gamma_0(0) + \frac{\Gamma_{LO}}{\exp\left(\frac{\Theta_{LO}}{T}\right) - 1}, \tag{5}$$

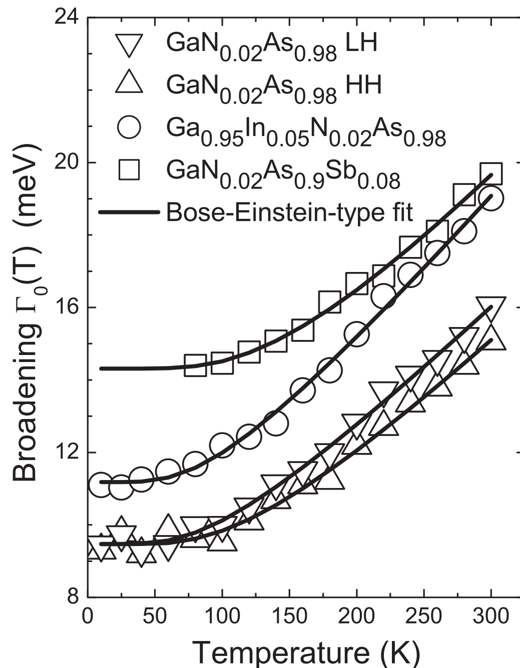


FIG. 5. Temperature dependencies of broadening of band-to-band transitions determined from PR measurements for as-grown $GaN_{0.02}As_{0.98}$, $Ga_{0.95}In_{0.05}N_{0.02}As_{0.98}$, and $GaN_{0.02}As_{0.90}Sb_{0.08}$ layers together with fits by the Bose-Einstein formula.

where $\Gamma_0(0)$ is the broadening mechanism due to intrinsic lifetime, electron-electron interaction, impurity, dislocation, and alloy scattering effects, $\Gamma_{LO}$ is the electron longitudinal-optical (LO) phonon coupling constant, and $\Theta_{LO}$ is the LO phonon temperature. Our experimental data have been fitted by Eq. (5) and the fitting curves are shown by solid lines in Fig. 5. The determined Bose-Einstein parameters are given in Table II.

In general, we found that the $E_0(T)$ and $\Gamma_0(T)$ and the parameters describing their variation are very similar to those which are reported for the corresponding N-free materials,[32] except the $\Gamma_0(0)$ parameter which increases with the nitrogen content due to the alloying effect, as expected. In other words, 2% of nitrogen atoms in a III-V host do not significantly influence the temperature dependence of the energy gap. Previous reports derived a reduced dependence of the band-gap energy of diluted nitrides with temperature as compared to their N-free counterpart.[17–22] It is worth noting that these works were based on PL measurements corrected from carrier localization energy at low temperatures. We believe that the discrepancy with our results is due to an inaccuracy in the estimate of the carrier localization from PL measurements. This estimate is especially difficult if the localized emission is observed up to the higher-temperature regime, e.g., up to 150 K. In this case, the application of absorptionlike techniques (e.g., photoreflectance) is the best approach to determine the temperature dependence of energy gap for III-V-N alloys. The increase of $\Gamma_0(0)$ parameter for N-containing alloys is attributed to alloy inhomogeneities and/or a short range clustering of atoms, which in our samples are quite small. It is worth noting that these inhomogeneities in III-V-N alloys as well atom clustering can be much larger and therefore the LH-HH splitting is often not observed; see, for example, Refs. 42 and 43.

TABLE II. Bose-Einstein parameters extracted from fitting of PR data shown in Fig. 5 by Eq. (5).

| Sample | $\Gamma_0$ (meV) | $\Gamma_{LO}$ (meV) | $\Theta_{LO}$ (K) |
|---|---|---|---|
| $GaN_{0.02}As_{0.98}$ | | | |
| LH | 9.47 | 13.1 | 361 |
| HH | 9.48 | 10.2 | 282 |
| $Ga_{0.95}In_{0.05}N_{0.02}As_{0.98}$ | 11.2 | 11.8 | 275 |
| $GaN_{0.02}As_{0.90}Sb_{0.08}$ | 14.3 | 19.2 | 457 |

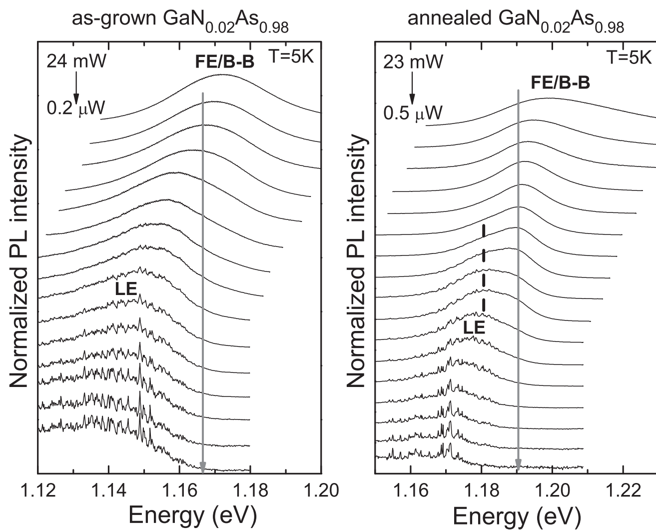


FIG. 6. $\mu$PL spectra measured at various excitation powers for as-grown (left panel) and annealed (right panel) $GaN_{0.02}As_{0.98}$ layers. The vertical line shows the energy gap determined from PR measurements.

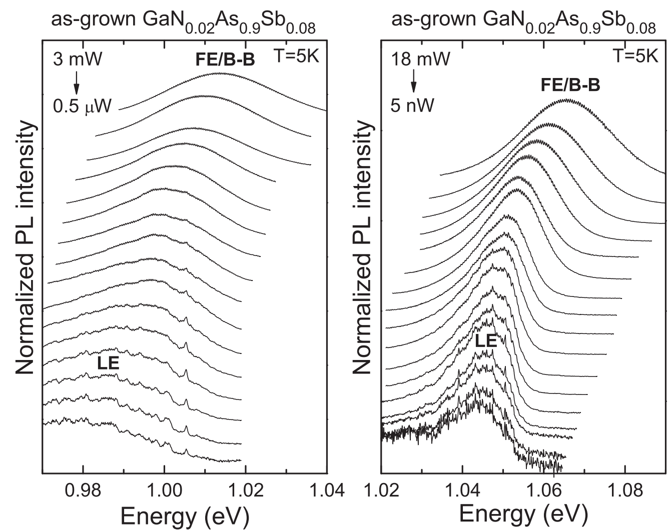


FIG. 8. $\mu$PL spectra measured at various excitation powers for as-grown (left panel) and annealed (right panel) $GaN_{0.02}As_{0.90}Sb_{0.08}$ layers.

### C. Microphotoluminescence studies of localized emission

Figures 6–8 show $\mu$PL spectra measured at various excitation conditions and low temperature for the as-grown and annealed $GaN_{0.02}As_{0.98}$, $Ga_{0.95}In_{0.05}N_{0.02}As_{0.98}$, and $GaN_{0.02}As_{0.90}Sb_{0.08}$ layers. In general, the power dependencies of $\mu$PL spectra are very similar for the three alloys. Sharp PL lines can be resolved at low excitation conditions. These lines are much better resolved for $GaN_{0.02}As_{0.98}$ and $Ga_{0.95}In_{0.05}N_{0.02}As_{0.98}$ alloys than for $GaN_{0.02}As_{0.90}Sb_{0.08}$. By moving out and then bringing back the excitation spot at a given position, we verified that the sharp spectra are reproducible at a given sample location. Thus, the whole fine structure of this main PL band is specific to the particular position on the sample and cannot be related to our measurement system. The very important observation is that these lines show no spectral shift with increasing excitation power; however, the sharp features smeared out. We attribute these sharp lines to localized excitons (LEs). At higher excitation, more LEs are created. They contribute to the emission spectrum until the individual lines cannot be resolved because their number becomes too large. For as-grown samples, the envelope of the whole emission band blueshifts with the increase in the excitation power and an additional broad emission band appears at the high-energy side. For the annealed $GaN_{0.02}As_{0.98}$ and $Ga_{0.95}In_{0.05}N_{0.02}As_{0.98}$ samples, it is also visible that at specific excitation conditions two emission bands become observable; see $\mu$PL spectra at the vertical dashed line. The lower-energy band is also observed at low excitation conditions and is composed of sharp PL lines whereas the higher-energy band is smooth. For each sample, the peak energy of the smooth band corresponds to the transition observed in the corresponding PR spectrum (Fig. 2). Since PR is insensitive to localized states, this peak is unambiguously attributed to the free exciton transition. At high excitation, this free exciton emission dominates the $\mu$PL spectra. The energy gap determined from PR measurements at 10 K is marked in Figs. 6–8 by vertical lines. These vertical lines are located below the PL peak measured at the highest excitation since, in this condition, free carriers with $\boldsymbol{k} \neq 0$ can contribute in the recombination process. It means that the measurements that are just $\mu$PL (or PL) without any support from the absorptionlike technique are insufficient to study the optical transitions between localized and delocalized states.

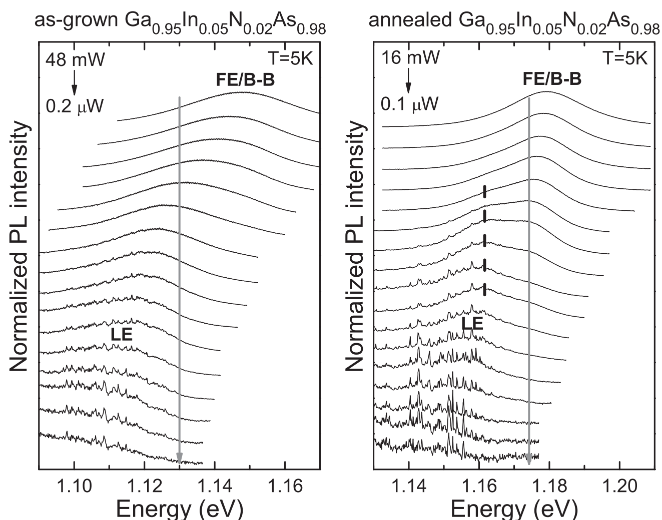


FIG. 7. $\mu$PL spectra measured at various excitation powers for as-grown (left panel) and annealed (right panel) $Ga_{0.95}In_{0.05}N_{0.02}As_{0.98}$ layers. The vertical line shows the energy gap determined from PR measurements.

We conclude that the smooth PL band at the higher-energy side is associated with delocalized states, namely, free exciton and/or band-to-band recombination. The sharp PL lines are separated from the energy gap by ~10–20 meV. Hence, they are attributed to the localized exciton recombination. In macro-PL spectra, the localized exciton recombination is also observed just below the energy gap (see the LE band in Fig. 1). In both micro- and macro-PL, this LE band shifts to blue when the excitation power is increased. This reflects the progressive

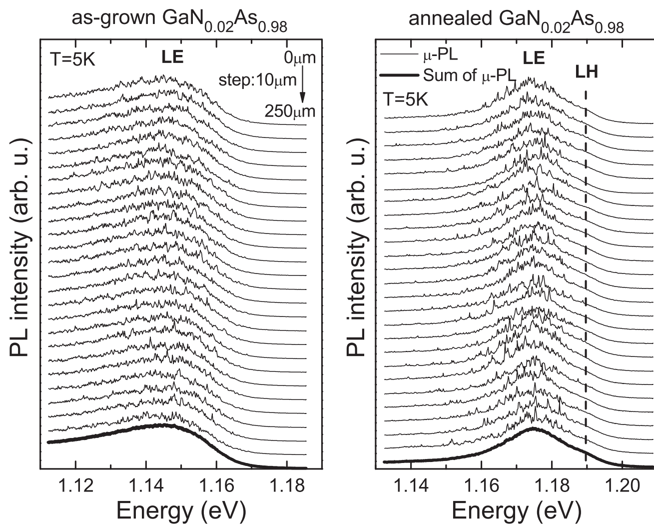


FIG. 9. $\mu$PL spectra measured along a line with a step of 10 $\mu$m and excitation power of 10 $\mu$W for as-grown (left panel) and annealed (right panel) $GaN_{0.02}As_{0.98}$ layers. The thick solid line represents the normalized sum of all $\mu$PL spectra shown above this line.

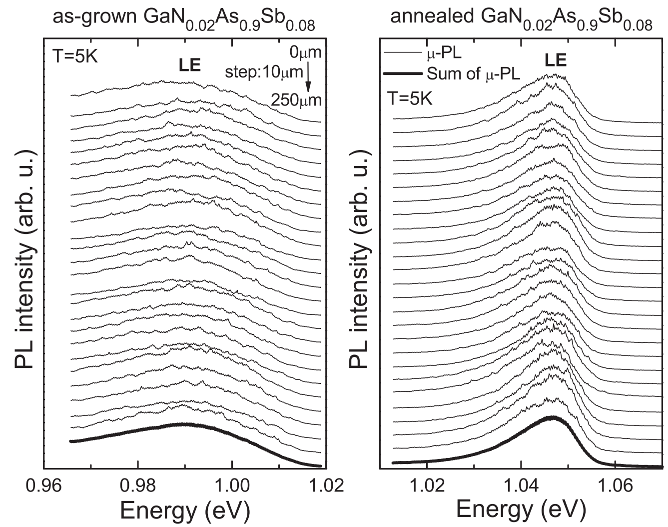


FIG. 11. $\mu$PL spectra measured along a line with a step of 10 $\mu$m and excitation power of 10 $\mu$W for as-grown (left panel) and annealed (right panel) $GaN_{0.02}As_{0.90}Sb_{0.08}$ layers. The thick solid line represents the normalized sum of all $\mu$PL spectra shown above this line.

filling of the localized states, until they become saturated. Then, the contribution of free excitons grows and becomes dominant. A further blueshift is eventually observed due to the contribution of free carrier recombination with $\boldsymbol{k} \neq 0$.

Several $\mu$PL spectra were measured on each sample, after changing the position of the excitation spot (the diameter of the laser spot is below 2 $\mu$m) along a straight line with 10-$\mu$m steps (Figs. 9–11). At each position, the set of sharp lines is different while the overall band extends over the same energy range. It evidences that individual LEs can be resolved in our $\mu$PL conditions. This is due to the small volume probed in that case. Many localized excitons coexist with various localization energies. When the probe size is too large, as in the macro-PL condition, the sharp peaks become blurred. This effect is well illustrated by summing several $\mu$PL spectra taken at different spatial position of the same sample (see bold line in Figs. 9–11 and details in figure captions). The result reasonably reproduces the smooth LE band of the macro-PL spectrum.

Now, we examine the impact of postgrowth annealing on the optical quality of the dilute nitride layers. For the three alloys, the whole LE band is narrowed after annealing (Figs. 9–11). Moreover, for the $GaN_{0.02}As_{0.98}$ and the $Ga_{0.95}In_{0.05}N_{0.02}As_{0.98}$ samples, the number of sharp lines is decreased upon annealing (Fig. 12). This behavior is not clearly observed for the $GaN_{0.02}As_{0.90}Sb_{0.08}N_{0.02}$ layer which shows an opposite tendency: Sharp features are more visible after annealing. We have already mentioned that the individual LE contributions in the as-grown $GaN_{0.02}As_{0.90}Sb_{0.08}$ sample are not well resolved in our $\mu$PL measurements. A too high density of LE can be at the origin of this observation. A

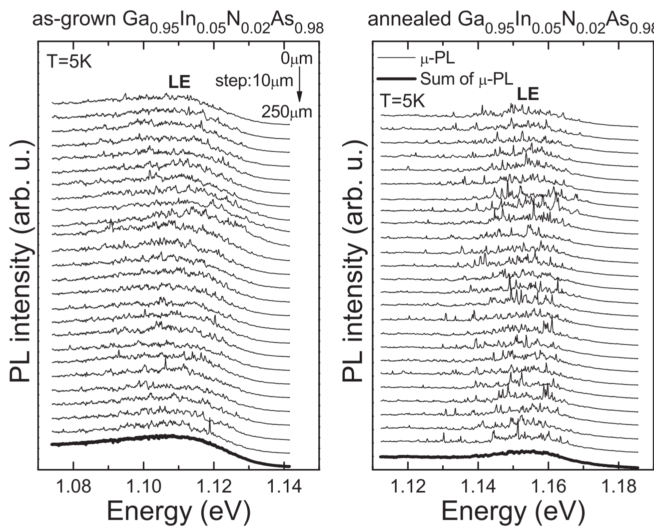


FIG. 10. $\mu$PL spectra measured along a line with a step of 10 $\mu$m and excitation power of 10 $\mu$W for as-grown (left panel) and annealed (right panel) $Ga_{0.95}In_{0.05}N_{0.02}As_{0.98}$ layers. The thick solid line represents the normalized sum of all $\mu$PL spectra shown above this line.

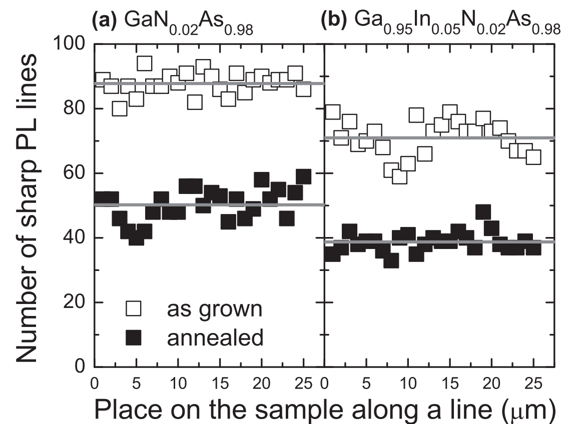


FIG. 12. The number of sharp PL lines calculated for each $\mu$PL spectrum measured for as-grown and annealed (a) $GaN_{0.02}As_{0.98}$ and (b) $Ga_{0.95}In_{0.05}N_{0.02}As_{0.98}$ layers along a line; see Figs. 9 and 10.

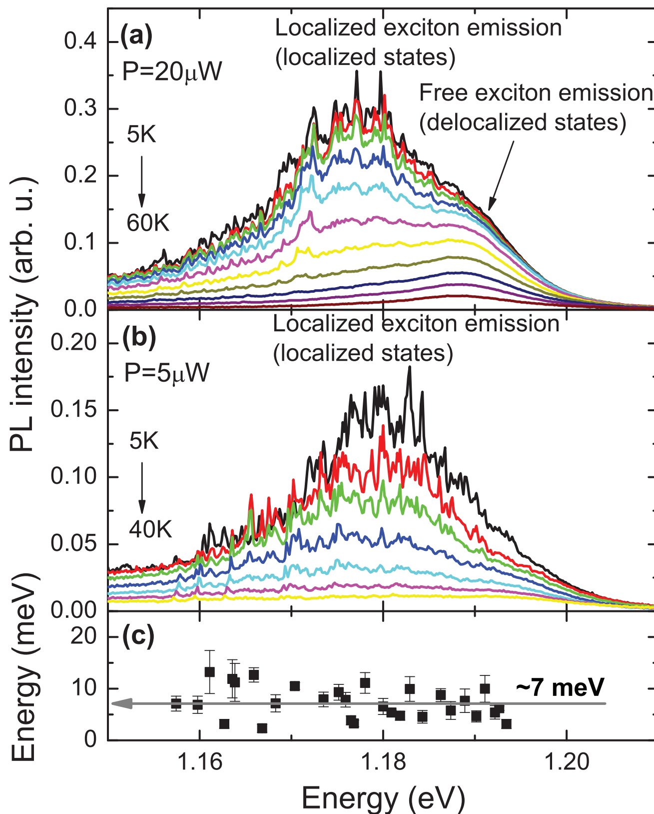


FIG. 13. (Color online) Temperature dependence of $\mu$PL spectra measured at the excitation power of (a) 20 $\mu$W and (b) 5 $\mu$W for the annealed $GaN_{0.02}As_{0.98}$ layer together with (c) activation energies determined for individual sharp PL lines observed in panel (b).

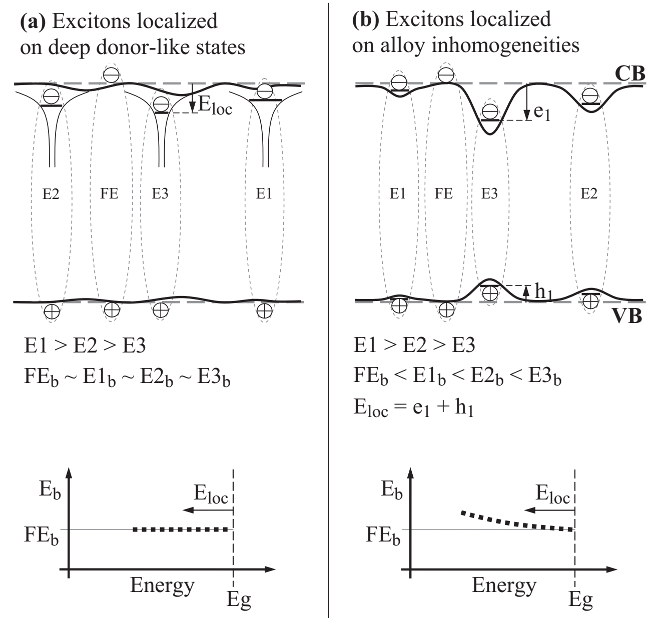


FIG. 14. (Color online) Sketch of excitons localized on deep donorlike states (a) and alloy inhomogeneities (b) together with the expected distribution of exciton binding energy ($E_b$) for the two types of excitons.

decrease of the LE density upon annealing could then reveal the sharp lines related to the remaining LE. These features indicate that the optical quality of the $GaN_{0.02}As_{0.90}Sb_{0.08}$ alloy is significantly different from that of the $GaN_{0.02}As_{0.98}$ and $Ga_{0.95}In_{0.05}N_{0.02}As_{0.98}$ alloys.

As discussed above, these excitons can be localized by alloy fluctuations and/or by deep donor (acceptor)-like states. For excitons localized on alloy fluctuations (i.e., excitons in quantum dots formed by alloy fluctuations), an enhancement of exciton binding energy is expected since the quantum confinement enhances the electron-hole attraction. This enhancement should scale with the depth of the potential minima associated with these alloy fluctuations. Therefore, a spectral dispersion of activation energy should be observed for such excitons. For excitons localized on deep donor (acceptor)-like states, the activation energy is not expected to vary since this energy results from the electron-hole attraction which is constant for such excitons. To investigate this question, we have determined the activation energies of individual lines from $\mu$PL measurements performed at various temperatures, using the approach presented in Ref. 15. The spectra obtained for the annealed $GaN_{0.02}As_{0.98}$ layer are shown in Fig. 13. In this particular case, the activation energy does not change with the localization energy: Within the experimental errors, the intensities of every sharp PL line present identical thermal quenching. The same behavior was observed for the $Ga_{0.95}In_{0.05}N_{0.02}As_{0.98}$ sample. It suggests that the main origin of these sharp lines is related to excitons localized on deep donor (acceptor)-like states for these two alloys. Indeed, the thermal quenching of their LE lines is governed by the Coulomb attraction between electrons and holes in bulk and homogeneous material.[15] In the case of the $GaN_{0.02}As_{0.90}Sb_{0.08}$ sample, the activation energy of individual sharp lines cannot be determined since they are not well resolved. Instead, we measured the activation energy for the whole LE band and found a value significantly larger than the activation energy obtained for the sharp lines in Ga(In)NAs alloys (i.e., 15 meV compared to 7 meV). It is worth noting that the activation energy for the whole LE band in $GaN_{0.02}As_{0.98}$ and $Ga_{0.95}In_{0.05}N_{0.02}As_{0.98}$ alloys is very similar to the average activation energy determined for individual sharp lines as should be expected since no spectral dispersion of activation energies is observed for sharp PL lines in these samples. It means that this larger activation energy suggests a different character of localization for the excitons in $GaN_{0.02}As_{0.90}Sb_{0.08}$. For this alloy, we invoke alloy inhomogeneities[11,12] producing potential fluctuations which can confine the excitons efficiently. The excess of activation energy is probably due to the quantum confinement in the potential fluctuations. Therefore, we believe that the LE emission observed for the $GaN_{0.02}As_{0.90}Sb_{0.08}$ sample is mainly due to excitons localized by alloy inhomogeneities. However, excitons localized on deep donor (acceptor)-like states are also present in this sample, and therefore some of the $\mu$PL spectra measured for the annealed $GaN_{0.02}As_{0.90}Sb_{0.08}$ sample possess sharp lines like those observed in $\mu$PL spectra of $GaN_{0.02}As_{0.98}$ and $Ga_{0.95}In_{0.05}N_{0.02}As_{0.98}$ samples, but this channel of recombination is not dominating in this sample.

Figures 14(a) and 14(b) schematically illustrate excitons localized on deep donorlike states and alloy inhomogeneities, respectively. The spectral dispersion of excitons localized on

alloy fluctuations is related to various sizes and contents of a given fluctuation. Such a potential fluctuation can enhance the binding energy of exciton confined on this fluctuation while the binding energy of excitons localized on deep donor (acceptor)-like states is expected to be constant and close to free exciton binding energy ($FE_b$) in this material. However, the spectral position of excitons localized on deep donorlike states of the same structural origin can vary in some range due to energy-gap fluctuations as shown in Fig. 14(a). When the thermal energy is higher than this attraction, electrons (holes) are still localized by deep donors (acceptors) but they cannot recombine radiatively since no hole (electron) is near the deep donor (acceptor) state. It means that the carriers localized by deep donors (acceptors) recombine nonradiatively when the thermal energy is higher than the free exciton binding energy. The source of deep donor (acceptor)-like states can be N-related point defects as well as point defects and impurities typical for the matrix material. For excitons confined on alloy fluctuations the Coulomb attractions between electrons and holes are stronger and hence they can be observed at higher temperatures. Moreover, carriers localized on such alloy inhomogeneity can recombine radiatively even if the thermal energy is larger than the exciton binding energy.

Alloy fluctuations and deep donor (acceptor)-like states influence the optical quality of III-V-N alloys in different ways. Alloy fluctuations with no other structural defect do not influence the internal quantum efficiency of PL. Conversely, the presence of deep donor (acceptor)-like states can be an important source of nonradiative recombination at room temperature. The two might coexist with variable weighting in the dilute nitrides alloys. An increase in the number of point defects without change in alloy fluctuations always leads to the reduction of the PL intensity. Conversely, an increase of alloy inhomogeneities without change in the concentration of point defects does not produce a degradation of the integrated PL intensity. If nonradiative centers coexist with alloy fluctuations, the latter can even reduce nonradiative recombination: The carriers localized by alloy fluctuations cannot diffuse toward the nonradiative centers. This situation is reported for the GaInN alloys which contain composition inhomogeneities as well as dislocations and other structural imperfections. Despite a high density of these structural defects, this GaInN alloy can emit a strong PL intensity, even at room temperature.[44,45]

Among the three samples investigated in this paper, the near-band-edge PL emission at room temperature is the strongest for the $GaN_{0.02}As_{0.90}Sb_{0.08}$ alloy. This suggests that either the density of nonradiative centers is smaller in this alloy, or their influence is reduced by the presence of stronger alloy fluctuations. The fact that the intensity of DT-VB recombination for $GaN_{0.02}As_{0.90}Sb_{0.08}$ is much weaker than for the two other alloys (see Fig. 1) indicates that the GaNAsSb alloy contains a lower concentration of deep donor (acceptor) states. On the other hand, our comparison of the three samples evidences that the excitons are more efficiently trapped in the alloy fluctuations of GaNAsSb. Therefore, the combination of these two characteristics could explain the stronger PL emission of this alloy.

Obtained results and analysis for single samples of three alloys clearly suggest that the formation of native point defects in dilute nitrides depends on the III-V host. GaAs and GaInAs hosts seem to be very similar whereas the GaAsSb host differs very significantly from the two previous hosts. Moreover it is expected that the optical activity of native defects in the three alloys is different. The energy-gap inhomogeneities in the GaAsSb host are larger than in Ga(In)As hosts and, therefore, energy-gap inhomogeneities in $GaN_{0.02}As_{0.90}Sb_{0.08}$ alloy are also much larger than in $GaN_{0.02}As_{0.98}$ and $Ga_{0.95}In_{0.05}N_{0.02}As_{0.98}$ alloys; this conclusion is confirmed by larger broadening of PR resonances for $GaN_{0.02}As_{0.90}Sb_{0.08}$. Because of this the presence of native point defects including N-related defects can be manifested with a weaker activity due to stronger carrier localization. A similar effect is observed in GaInN alloys.[44,45]

Finally, it is not excluded that a donor-acceptor pair (DAP) recombination is also present for these alloys. But it is surely excluded that the whole band of sharp PL lines has DAP character since no phonon replicas are observed for this band and the shape of this band is unusual for DAP recombination.

### D. Monte Carlo simulations of microphotoluminescence spectra

Changes observed in $\mu$PL spectra can be reproduced by Monte Carlo simulations within the model of hopping excitons.[46] After other authors,[47,48] we assume that excitons behave like noninteracting single particles which can be trapped by localization potentials due to the energy dissipation process, i.e., they migrate between localization potentials with a given probability via phonon emission (hopping to states with lower energy) and phonon absorption (hopping to states with higher energy). The energies of the localized states are chosen in such a way that they create an exponential density of states (DOS). An exciton trapped by the localization center can recombine radiatively, hop to the extended states or hop to another localization center. A detailed description of Monte Carlo simulations of $\mu$PL spectra is given in Ref. 46. In this section essential points of our approach to simulate $\mu$PL spectra are described. Next, a few examples of simulated $\mu$PL spectra are presented and discussed in the context of experimental data reported in this paper. We focus on simulations of $\mu$PL spectra with different carrier generation rate (it corresponds to $\mu$PL measurements with different excitation power), various temperatures, and different densities of localization centers (e.g., point defects).

The key issue in our model is that we assume that the same localization center is radiative or nonradiative depending on the temperature. At low temperatures, when the thermal energy is smaller than the exciton binding energy, such a center works as a radiative center but if the temperature is higher than the exciton binding energy this center works as a nonradiative center. Such an assumption results from recent experimental studies of the activation energy of individual exciton lines for GaInNAs alloys.[15] We observed that the activation energy for localized excitons does not change with the localization energy and is equal to the electron-hole attraction energy (Fig. 13). Taking into account this fact we assume that the nonradiative recombination rate $\nu_{nr}$ is described by the expression

$$\nu_{nr} = \nu_d \exp\frac{-\varepsilon_b}{kT}, \qquad (6)$$

where $\nu_d$ is the rate of exciton dissociation (nonradiative recombination) and $\varepsilon_b$ is the energy of electron-hole attraction in Ga(In)NAs. This energy is assumed to be $\varepsilon_b = 7$ meV according to the analysis in Fig. 13 and Ref. 15. Another modification that we have done in comparison to previous simulations[47,48] is to take into account saturation effects and emission from delocalized states; see details in Ref. 46. Finally, the following events can happen in our simulations:

(i) A free exciton can recombine radiatively, can dissociate, or can be captured by an unoccupied localized center with the rate

$$\nu_{\mathrm{cap}} = \nu_0 \frac{N_f}{N}, \tag{7}$$

where $\upsilon_o$ is the characteristic frequency of the hopping process, $N_f$ is the number of unoccupied localized states, and $N$ is the total number of localized states. The free exciton recombines with a random energy which is described by the Gaussian distribution resulting from alloy inhomogeneities.

(ii) A localized exciton can recombine radiatively with the rate given by $\nu_r = \tau_0^{-1}$ ($\tau_0$ is the exciton recombination time), recombine nonradiatively with the rate given by Eq. (6), hop to the extended states with the rate given by $\nu_a = \nu_0 \exp(-\frac{\varepsilon_i}{kT})$, or hop to another unoccupied localization center with the rate given by the Miller-Abrahams formula $\upsilon_{ij} = \upsilon_0 \exp(-\frac{2r_{ij}}{\alpha} - \frac{\varepsilon_j - \varepsilon_i + |\varepsilon_j - \varepsilon_i|}{2kT})$, where $\varepsilon_i$ and $\varepsilon_j$ are the localization energy of said $i$ and $j$, $r_{ij}$ is the distance between them, and $\alpha$ is the decay length of the exciton center of mass wave function.[46–48] The radiative emission from a localized state is described by a PL peak with a Lorentzian line shape.

In the previous work[46] we used an appropriate algorithm to take into account the saturation effect. We created a list which contains a given number ($n$) of free excitons at time $t = 0$. Next we took the first exciton from the list and determined the type of process for this exciton and the time for the next process for this exciton. After this procedure excitons were sorted in the list according to the time of the next process. Such an exciton was removed from the list if the recombination process took place. This procedure was repeated until all excitons recombined. It is worth noting that this approach corresponds more to a pulse laser excitation rather than a continuous wave (cw) excitation, which is used in the present $\mu$PL measurements. In order to make these simulations closer to cw excitation conditions, the above-described algorithm can be easily modified by changes in the preparation of the exciton list. Instead of creating all free excitons at time $t = 0$ we create a list which contains excitons uniformly distributed according to the time of creation (appearing as free excitons). The ratio of number of excitons $n$ created in time interval $\Delta t$ is a generation rate $G$.

For a given distribution of localization centers, simulations were repeated many times in order to obtain reliable results. The needed parameters for our simulations are $\tau_0\nu_0$, $\tau_0\nu_d$, and $\frac{N\alpha^3}{L^3}$. To estimate the value of $\tau_0\nu_0$, we take $\nu_0$ equal to the Debye frequency ($\nu_0 = 10^{-13}$ s$^{-1}$) and the exciton lifetime in GaNAs and GaInNAs equal to 100 ps on the basis of time-resolved PL measurements.[49,50] This gives $\tau_0\nu_0 = 10^3$. The $\tau_0\nu_d$ parameter can be extracted from the PL measurements; see details in Ref. 46. For the low-temperature regime in dilute nitrides this parameter is in the range of 10–100,[51,52] and for our simulation this parameter is assumed to be 14 as in Ref. 46.

For localized states we assume an exponential DOS,

$$\mathrm{DOS}(\varepsilon) = \frac{N/L^3}{\varepsilon_0} \exp\left(-\frac{\varepsilon}{\varepsilon_0}\right), \tag{8}$$

with $\varepsilon_0 = 10$ meV, which is determined according to the rule $\Delta\varepsilon = 3\varepsilon_0$,[53] where $\Delta\varepsilon$ is the full width at half maximum of the PL peak. $L$ is the size of the cubic volume and $N$ is the number of localized states in this volume. We performed simulations for various $N$ (i.e., various values of $\frac{N\alpha^3}{L^3}$, where $\alpha$ is the same decay length of the exciton wave function which appears in the Miller-Abrahams formula; see details in Refs. 46–48).

In order to generate $\mu$PL spectra, we sum all the recombination processes, which are described by a Lorentzian line with broadening $\gamma = 0.7$ meV for the localized exciton emission and a Gaussian line with broadening $\sigma = 10$ meV for the free exciton emission. These broadening values are consistent with the experimental data reported above. The large broadening of the free exciton recombination line is due to inhomogeneities in III-V-N alloys.

Figure 15 shows $\mu$PL spectra simulated for different generation rate $G$. It is clear that at large $G$, the PL spectrum is dominated by the free exciton recombination (this contribution is represented by the short-dashed red line in Fig. 15). Besides the main PL peak, a small contribution of localized exciton recombination is observed at the low-energy side. When the number of injected carriers is decreased, the free exciton recombination disappears and the spectrum is dominated by sharp lines which are associated with the recombination of localized excitons. These simulations reproduce fairly well

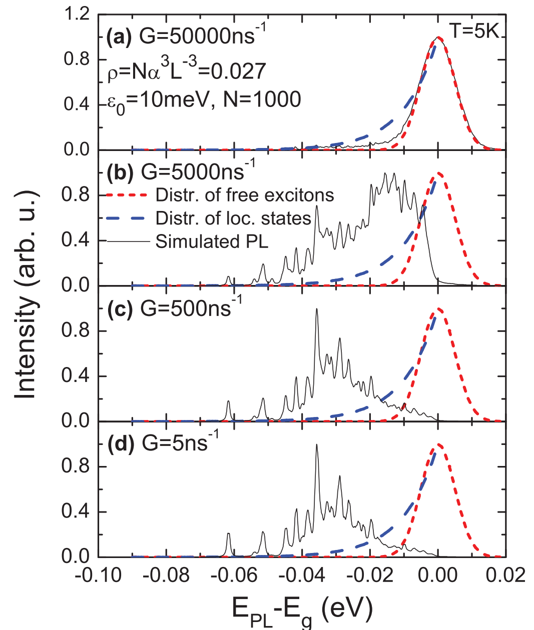


FIG. 15. (Color online) Theoretical simulations of $\mu$PL spectra obtained for various generation rate (a) $G = 50\,000$ ns$^{-1}$, (b) $G = 5000$ ns$^{-1}$, (c) $G = 500$ ns$^{-1}$, and (d) $G = 5$ ns$^{-1}$. Simulations were performed at $T = 5$ K for $N\alpha^3/L^3 = 0.027$ ($N = 1000$); the dashed blue lines represent the exponential tail of DOS with $\varepsilon_0 = 10$ meV; the short-dashed red lines represent Gaussian distribution of free exciton transition with the broadening $\sigma = 10$ meV. The simulated $\mu$PL spectra are normalized to 1 for better visualization.

our experimental $\mu$PL spectra showing sharp PL lines at low excitation power (Figs. 6–8). In the low carrier injection regime ($G\tau_0 < N$), the evolution of $\mu$PL spectra is related to hopping of excitons between localized states. This phenomenon is random, and due to the hopping process the DOS (see the dashed red line) is not an envelope of the PL spectrum. When the generation rate is large ($G\tau_0 \gg N$) the hopping process is strongly reduced since most of the localized states are occupied. The exciton recombines from its localized state or hops to the extended states and recombine as a free exciton.

Besides the generation rate $G$, the shape of the PL spectra depends on the number of localizing states. This number can change from sample to sample due to different growth conditions, the change of host matrix, and the postgrowth treatment (e.g., annealing). In the Monte Carlo simulations of $\mu$PL spectra the number of localizing states is represented by the $N$ parameter. Figure 16 shows the influence of $N$ parameter on $\mu$ PL spectra obtained for low (left panel) and large (right panel) exciton generation rates. It is clearly visible that the band of sharp PL lines is enhanced when the number of localizing potentials ($N$ parameter) is increased. This effect is much more visible for larger exciton generation since the two parameters ($G\tau_0$ and $N$) are more comparable in this case. It is worth noting that in some regimes of exciton generation and numbers of localizing potentials it is rather difficult to make conclusions about the number of localizing potentials from experimental data (i.e., compare in which sample the number of localizing centers is larger). In these regimes of $G$ and $N$ parameters the $\mu$PL spectra look very similar due to the random character of energy transfer to localized states. It means that the number of sharp lines does not correspond directly to the sample quality since the localizing centers, which are associated with particularly narrow PL lines, can contribute in the emission process with different magnitudes. However if the number of localizing centers differs by an order or a few orders it should be possible to recognize some difference in $\mu$PL spectra. The main difference lies in the "effective" spectral position of the band of sharp lines. For samples with larger numbers of localizing centers this band is more strongly shifted to red (i.e., the Stokes shift is larger). This effect is clearly observed in our simulations (see Fig. 16) and experimental data if the as-grown and annealed samples are compared (see Figs. 6 and 7). The increase of redshift is caused by the enhancement of the hopping process. When the density of localizing states increases excitons can more easily achieve more deeply situated localizing states. A more comprehensive discussion of this effect can be found in Ref. 54.

The other experimental observation, which can be reproduced by Monte Carlo simulations, is the fast thermal quenching of sharp PL lines. In our simulations, it is very easy to take the influence of temperature into account since $kT$ energy is directly in our equations; see Eq. (6) and Ref. 46. An example is shown in Fig. 17. The simulation reproduces the experimental observation of Fig. 13: When the temperature is increased, the intensity of each sharp PL peak decreases and the relative intensities between individual peaks is not changed.

It is worth noting that the results of simulations presented in this work are qualitatively very similar to those reported

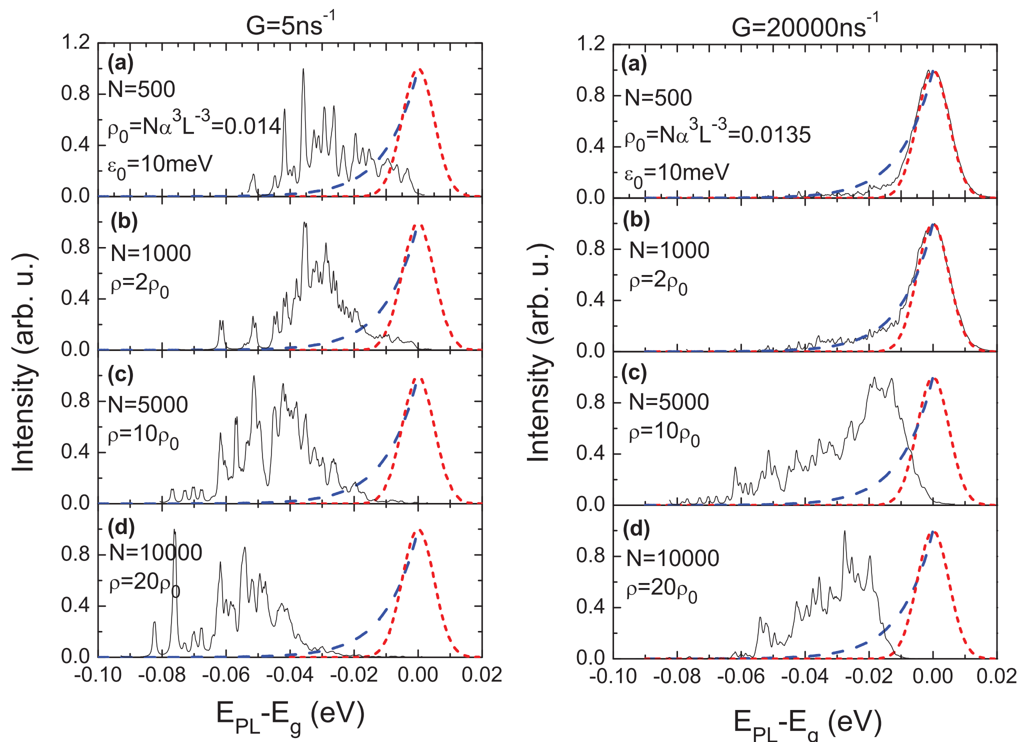


FIG. 16. (Color online) Theoretical simulations of $\mu$PL spectra obtained for low (left panel) and high (right panel) carrier injection for systems with various concentrations of localizing centers which are represented by $N$. Simulations were performed at $T = 5$ K for $N = 500$, 1000, 5000, and 10 000; the dashed blue lines represent the exponential tail of DOS with $\varepsilon_0 = 10$ meV; the short-dashed red lines represent Gaussian distribution of free exciton transition with the broadening $\sigma = 10$ meV.

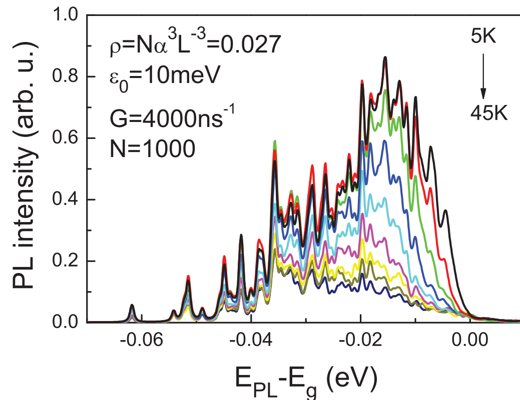


FIG. 17. (Color online) Theoretical simulations of temperature dependence of $\mu$PL spectra obtained for carrier injections of $G = 4000\ \mathrm{ns}^{-1}$. Simulations were performed for $N\alpha^3/L^3 = 0.027$ ($N = 1000$).

in Ref. 46 despite the fact that the previous simulations were performed for conditions corresponding to a pulse injection of carriers (a pulse excitation), which can be far from cw excitation. Any significant differences between the present and previous simulations are observed since the time constant describing the carrier capture and hopping process is much smaller than the recombination time. In the short time after the pulse excitation, excitons are captured by localizing states and these states stay occupied for a relatively long time, so the remaining free excitons cannot be captured by these states and therefore they recombine as free excitons. The saturation effect looks very similar for cw excitation conditions in some range of excitation intensity, i.e., some of the excitons are captured by localizing states and they saturate these states. Excitons that are generated later cannot be captured by saturated states and therefore they recombine as free excitons. The difference in this two excitation modes would be clearly visible in the time-resolved PL experiment; however, in the time-integrated PL experiment the method of sample excitation does not change the character of the $\mu$PL spectrum.

## IV. SUMMARY

The temperature dependence of the energy gap has been determined for $GaN_{0.02}As_{0.98}$, $Ga_{0.95}In_{0.05}N_{0.02}As_{0.98}$, and $GaN_{0.02}As_{0.90}Sb_{0.08}$ alloys from PR measurements, which are absorptionlike and hence not sensitive to localized states. In addition, the free exciton binding energies in $GaN_{0.02}As_{0.98}$ and $Ga_{0.95}In_{0.05}N_{0.02}As_{0.98}$ layers have been determined from PR measurements in a low-temperature range. These energies are $4.5 \pm 0.5$ and $6.5 \pm 0.5$ meV for the LH and HH exciton, respectively, in $GaN_{0.02}As_{0.98}$ and $8 \pm 2$ eV for the HH exciton in $Ga_{0.95}In_{0.05}N_{0.02}As_{0.98}$.

Optical transitions from localized states have been clearly observed in PL and $\mu$PL spectra. Their nature has been determined on the basis of $\mu$PL measurements at various excitation powers and temperatures and their comparison with PR measurements. Three PL bands have been identified in macro-PL spectra for the three alloys. The first band is observed ~0.2–0.4 eV below the energy gap and is due to DT-VB recombination. The second band is observed ~10–40 meV below the energy gap and comes from the emission of localized excitons. This emission was studied in detail in $\mu$PL. It is concluded that two types of localized excitons exist in these layers: (i) excitons localized on deep donor (acceptor)-like states and (ii) excitons localized on alloy content fluctuations. The first type of exciton dominates in $GaN_{0.02}As_{0.98}$ and $Ga_{0.95}In_{0.05}N_{0.02}As_{0.98}$ layers whereas the second type of exciton dominates in the $GaN_{0.02}As_{0.90}Sb_{0.08}$ layer. The third band of emission is related to the free exciton and band-to-band recombination. This emission is clearly observed in $\mu$PL spectra at high excitation conditions.

Comparing PR, PL, and $\mu$PL spectra measured for the three layers, it is concluded that the $GaN_{0.02}As_{0.90}Sb_{0.08}$ alloy presents the largest compositional inhomogeneities and the lowest density of deep donor (acceptor)-like states. The room temperature PL intensity is much stronger for this alloy than for Ga(In)NAs alloys. These results indicate that the formation of native point defects, probably related to N, and their optical activity depend on the III-V host matrix. GaAs and GaInAs hosts seem to be very similar whereas the GaAsSb host contrasts with the two others.

## ACKNOWLEDGMENT

This work was partially performed under the MNiSzW Grant No. N202 258339.

*robert.kudrawiec@pwr.wroc.pl
†Present address: School of Electronic and Electrical Engineering, University of Leeds, Leeds LS2 9JT, United Kingdom.

[1] M. Henini, *Dilute Nitride Semiconductors* (Elsevier Ltd, Oxford, 2005).
[2] W. Shan, W. Walukiewicz, J. W. Ager III, E. E. Haller, J. F. Geisz, D. J. Friedman, J. M. Olson, and S. R. Kurtz, Phys. Rev. Lett. **82**, 1221 (1999).
[3] P. R. C. Kent and A. Zunger, Phys. Rev. B **64**, 115208 (2001).
[4] R. Kudrawiec, J. Misiewicz, Q. Zhuang, A. M. R. Godenir, and A. Krier, Appl. Phys. Lett. **94**, 151902 (2009).
[5] M. Kondow, K. Uomi, A. Niwa, T. Kitatani, S. Watahiki, and Y. Yazawa, Jpn. J. Appl. Phys., Part 1 **35**, 1273 (1996).
[6] S. R. Bank, B. Hopil, L. L. Goddard, H. B. Yuen, M. A. Wistey, R. Kudrawiec, and J. S. Harris, IEEE J. Quantum Electron. **43**, 773 (2007).
[7] J. S. Harris, Jr, R. Kudrawiec, H. B. Yuen, S. R. Bank, H. P. Bae, M. A. Wistey, D. Jackrel, E. R. Pickett, T. Sarmiento, L. L. Goddard, V. Lordi, and T. Gugov, Phys. Status Solidi B **244**, 2707 (2007).
[8] I. A. Buyanova, W. M. Chen, G. Pozina, J. P. Bergman, B. Monemar, H. P. Xin, and C. T. Tu, Appl. Phys. Lett. **75**, 501 (1999).
[9] R. Kudrawiec, G. Sek, J. Misiewicz, L. H. Li, and J. C. Harmand, Eur. Phys. J: Appl. Phys. **27**, 313 (2004).
[10] K. Matsuda, T. Saiki, M. Takahashi, A. Moto, and S. Takagishi, Appl. Phys. Lett. **78**, 1508 (2001).

[11]A. M. Mintairov, T. H. Kosel, J. L. Merz, P. A. Blabnov, A. S. Vlasov, V. M. Ustinov, and R. E. Cook, Phys. Rev. Lett. **87**, 277401 (2001).

[12]A. M. Mintairov, K. Sun, J. L. Merz, H. Yuen, S. Bank, M. Wistey, J. S. Harris, G. Peake, A. Egorov, V. Ustinov, R. Kudrawiec, and J. Misiewicz, Semicond. Sci. Technol. **24**, 075013 (2009).

[13]R. Kudrawiec, G. Sęk, J. Misiewicz, F. Ishikawa, A. Trampert, and K. H. Ploog, Appl. Phys. Lett. **94**, 011907 (2009).

[14]R. Kudrawiec, M. Latkowska, G. Sęk, J. Misiewicz, J. Ibáñez, M. Henini, and M. Hopkinson, Acta Phys. Pol. **116**, 930 (2009).

[15]M. Latkowska, R. Kudrawiec, G. Sęk, J. Misiewicz, J. Ibáñez, M. Henini, and M. Hopkinson, Appl. Phys. Lett. **98**, 131903 (2011).

[16]G. Patriarche, L. Largeau, J. C. Harmand, and D. Gollub, Appl. Phys. Lett. **84**, 203 (2004).

[17]H. Yaguchi, S. Kikuchi, Y. Hijikata, S. Yoshida, D. Aoki, and K. Onabe, Phys. Status Solidi B **228**, 273 (2001).

[18]M.-A. Pinault and E. Tournie, Appl. Phys. Lett. **78**, 1562 (2001).

[19]R. J. Potter, N. Balkan, H. Carrere, A. Arnoult, E. Bedel, and X. Marie, Appl. Phys. Lett. **82**, 3400 (2003).

[20]T. K. Ng, S. F. Yoon, W. K. Loke, and S. Wicaksono, J. Cryst. Growth **270**, 351 (2004).

[21]Q. X. Zhao, S. M. Wang, Y. Q. Wei, M. Sadeghi, A. Larsson, and M. Willander, Phys. Lett. A **341**, 297 (2005).

[22]F.-I. Lai, S. Y. Kuo, J. S. Wang, H. C. Kuo, S. C. Wang, H. S. Wang, C. T. Liang, and Y. F. Chen, J. Vac. Sci. Technol. A **24**, 1223 (2006).

[23]J-C. Harmand, L. Li, R. Mouillet, G. Ungaro, V. Sallet, L. Travers, G. Patriarche, L. Largeau, R. Kudrawiec, G. Sek, and J. Misiewicz, in *Dilute Nitride Semiconductors*, edited by M. Henini (Elsevier, Amsterdam, 2005), Chap. 15, pp. 471–493.

[24]R. Kudrawiec and J. Misiewicz, Rev. Sci. Instrum. **80**, 096103 (2009).

[25]P. J. Klar, H. Grüning, J. Koch, S. Schäfer, K. Volz, W. Stolz, W. Heimbrodt, A. M. Kamal Saadi, A. Lindsay, and E. P. O'Reilly, Phys. Rev. B **64**, 121203(R) (2001).

[26]R. Kudrawiec, G. Sek, J. Misiewicz, D. Gollub, and A. Forchel, Appl. Phys. Lett. **83**, 2772 (2003).

[27]R. Kudrawiec, E.-M. Pavelescu, J. Wagner, G. Sek, J. Misiewicz, M. Dumitrescu, J. Konttinen, A. Gheorghiu, and M. Pessa, J. Appl. Phys. **96**, 2576 (2004).

[28]V. Lordi, H. B. Yuen, S. R. Bank, M. A. Wistey, J. S. Harris, and S. Friedrich, Phys. Rev. B **71**, 125309 (2005).

[29]R. Kudrawiec, M. Latkowska, M. Welna, J. Misiewicz, M. Shafi, R. H. Mari, M. Henini, and W. Walukiewicz, Appl. Phys. Lett. **101**, 082109 (2012).

[30]R. Kudrawiec, G. Sek, J. Misiewicz, L. H. Li, and J. C. Harmand, Appl. Phys. Lett. **83**, 1379 (2003).

[31]R. Kudrawiec, M. Gladysiewicz, J. Misiewicz, H. B. Yuen, S. R. Bank, M. A. Wistey, H. P. Bae, and J. S. Harris, Jr., Phys. Rev. B **73**, 245413 (2006).

[32]I. Vurgaftman, J. R. Meyer, and L. R. Ram-Mohan, J. Appl. Phys. **89**, 5815 (2001).

[33]D. E. Aspnes, Surf. Sci. **37**, 418 (1973).

[34]R. Kudrawiec, J. Misiewicz, L. H. Li, and J. C. Harmand, AIP Conf. Proc. **772**, 291 (2005).

[35]Y. P. Varshni, Physica (Amsterdam) **34**, 49 (1967).

[36]P. Lantenschlager, M. Garriga, S. Logothetidis, and M. Cardona, Phys. Rev. B **34**, 2458 (1986).

[37]C. Skierbiszewski, I. Gorczyca, S. P. Łepkowski, J. Łusakowski, J. Borysiuk, and J. Toivonen, Semicond. Sci. Technol. **19**, 1189 (2004).

[38]R. Kudrawiec, M. Motyka, M. Gładysiewicz, J. Misiewicz, J. A. Gupta, and G. C. Aers, Solid State Commun. **138**, 365 (2006).

[39]K. Kornitzer, T. Ebner, K. Thonke, R. Sauer, C. Krichner, V. Schwegler, M. Kamp, M. M. Leszczynski, I. Grzegory, and S. Porowski, Phys. Rev. B **60**, 1471 (1999).

[40]D. Reynolds, D. Look, B. Jogai, C. Litton, G. Cantwell, and W. Harsch, Phys. Rev. B **60** 2340 (1999).

[41]P. Lautenschlager, M. Garriga, S. Logothetidis, and M. Cardona, Phys. Rev. B **35**, 9174 (1987).

[42]A. Nishikawa, R. Katayama, K. Onabe, and S. Shiraki, J. Cryst. Growth **251**, 427 (2003).

[43]W. Rudno-Rudzinski, R. Kudrawiec, J. Misiewicz, J. Derluyn, and I. Moerman, Phys. Status Solidi C **1**, 329 (2004).

[44]J. C. Zhang, D. S. Jiang, Q. Sun, J. F. Wang, Y. T. Wang, J. P. Liu, J. Chen, R. Q. Jin, J. J. Zhu, H. Yang, T. Dai, and Q. J. Jia, Appl. Phys. Lett. **87**, 071908 (2005).

[45]M. S. Jeong, Y.-W. Kim, J. O. White, E.-K. Suh, M. G. Cheong, C. S. Kim, C.-H. Hong, and H. J. Lee, Appl. Phys. Lett. **79**, 3440 (2001).

[46]M. Baranowski, M. Latkowska, R. Kudrawiec, and J. Misiewicz, J. Phys.: Condens. Matter **23**, 205804 (2011).

[47]O. Rubel, S. D. Baranovskii, K. Hantke, B. Kunert, W. W. Rühle, P. Thomas, K. Volz, and W. Stolz, Phys. Rev. B **73**, 233201 (2006).

[48]O. Rubel, M. Galluppi, S. D. Baranovskii, K. Volz, L. Geelhaar, H. Riechert, P. Thomas, and W. Stolz, J. Appl. Phys. **98**, 063518 (2005).

[49]R. A. Mair, J. Y. Lin, H. X. Jiang, E. D. Jones, A. A. Allerman, and S. R. Kurtz, Appl. Phys. Lett. **76**, 188 (2000).

[50]X. D. Luo, Z. Y. Xu, W. K. Ge, Z. Pan, L. H. Li, and Y. W. Lin, Appl. Phys. Lett. **79**, 958 (2001).

[51]H. D. Sun, S. Calvez, M. D. Dawson, J. A. Gupta, G. C. Aers, and G. I. Sproule, Appl. Phys. Lett. **89**, 101909 (2006).

[52]I. A. Buyanova, M. Izadifard, W. M. Chen, A. Polimeni, M. Capizzi, H. P. Xin, and C. W. Tu, Appl. Phys. Lett. **82**, 3662 (2003).

[53]H. Grüning, K. Kohary, S. D. Baranovskii, O. Rubel, P. J. Klar, A. Ramakrishnan, G. Ebbinghaus, P. Thomas, W. Heimbrodt, W. Stolz, and W. W. Rühle, Phys. Status Solidi C **1**, 109 (2004).

[54]M. Baranowski, M. Latkowska, R. Kudrawiec, and J. Misiewicz, Acta Phys. Pol. **120**, 899 (2011).